

Scale-Invariant Gradient Aggregation for Constrained Multi-Objective Reinforcement Learning

Dohyeong Kim¹ Mineui Hong¹ Jeongho Park¹ Songhwai Oh¹

Abstract

Multi-objective reinforcement learning (MORL) aims to find a set of Pareto optimal policies to cover various preferences. However, to apply MORL in real-world applications, it is important to find policies that are not only Pareto optimal but also satisfy pre-defined constraints for safety. To this end, we propose a constrained MORL (CMORL) algorithm called *Constrained Multi-Objective Gradient Aggregator (CoMOGA)*. Recognizing the difficulty of handling multiple objectives and constraints concurrently, CoMOGA relaxes the original CMORL problem into a constrained optimization problem by transforming the objectives into additional constraints. This novel transformation process ensures that the converted constraints are invariant to the objective scales while having the same effect as the original objectives. We show that the proposed method converges to a local Pareto optimal policy while satisfying the predefined constraints. Empirical evaluations across various tasks show that the proposed method outperforms other baselines by consistently meeting constraints and demonstrating invariance to the objective scales.

1. Introduction

Many real-world reinforcement learning (RL) applications involve multiple objectives. For example, in autonomous driving, vehicles must maintain fuel, avoid collisions, and reach their destination quickly. The presence of such multiple objectives has led to extensive studies of multi-objective RL (MORL) (Roijers et al., 2013), which aim to find a set of *Pareto-optimal* policies (Hayes et al., 2022) that are not dominated by any other policies, instead of finding a single optimal policy. This allows users to choose and utilize their preferred policy from the set without additional training.

¹Department of Electrical and Computer Engineering, Seoul National University. Correspondence to: Songhwai Oh <songhwai@snu.ac.kr>.

Preprint.

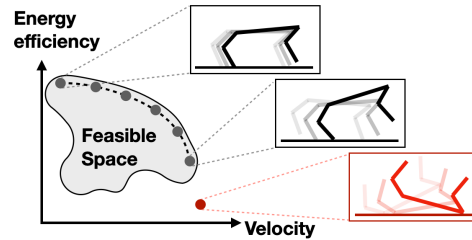


Figure 1: An example of constrained MORL (CMORL). The robot aims to maximize energy efficiency and velocity while maintaining its balance to avoid falling. To this end, CMORL finds a set of feasible policies that are not dominated by other policies and satisfy constraints, which are indicated as the dashed line.

In order to represent the set of Pareto optimal policies, it is common to use a concept called *preference* (Yang et al., 2019; Kyriakis & Deshmukh, 2022), which encodes the relative importance of the objectives. A preference-conditioned policy can then represent the set of policies.

A number of MORL algorithms (Désidéri, 2012; Yang et al., 2019; Basaklar et al., 2023) update the preference-conditioned policy by maximizing a scalarized reward, computed as the dot product of a given preference and rewards from the multiple objectives. However, such scalarization is sensitive to the scale of objectives. For example, if a particular reward among multiple rewards has a significant scale, the majority of the trained policy set will converge towards focusing on that reward, as observed in Section 6.5. Hence, despite training a set of policies, there may be no user-preferred policy in the set, as they tend to be clustered around high-scale rewards. For this reason, it is required to develop a scale-invariant MORL algorithm.

Additionally, in domains where safety is paramount, such as robotic control and autonomous driving, it is crucial to incorporate constraints into MORL to enhance safety assurance, an example of which is shown in Figure 1. A straightforward approach to reflect constraints in MORL is treating the constraints as other objectives and concurrently updating the preferences corresponding to those objectives to maintain them below thresholds, as done by (Huang et al., 2022). This approach exactly aligns with the Lagrangian method, which solves the Lagrange dual problem by updating policy and multipliers alternatively. However, the

Lagrangian method can make training unstable due to the concurrent update of policy and multipliers (Stooke et al., 2020; Kim & Oh, 2022). As the updates of the policy and multipliers influence each other, any misstep in either can make the training process diverge. Therefore, it is essential to incorporate constraints into MORL without additional optimization variables.

In this paper, we propose a constrained MORL (CMORL) algorithm that is scale-invariant and does not require any additional optimization variables. The primary component of our algorithm is *Constrained Multi-Objective Gradient Aggregator (CoMOGA)*, which calculates a policy gradient by aggregating the gradients of the objective and constraint functions. Instead of treating the constraints as new objectives like an existing CMORL method (Huang et al., 2022), CoMOGA transforms the objectives into extra constraints. This novel transformation process makes solving the CMORL problem simple and intuitive by removing the multi-objective components. The transformed constraints are designed to increase the objectives using the gradients of the objective functions. Since only the directional component of the gradient is used, they are invariant to the objective scales. Furthermore, to reflect a given preference, we set the threshold of the transformed constraints to be proportional to the preference value. CoMOGA finally calculates the policy gradient by solving the transformed problem using linear approximation within a local region of the policy parameter space. Under mild assumptions, we have shown that updating a policy using CoMOGA monotonically increases objectives corresponding to specific preferences while consistently satisfying the constraints. Thus, constraints can be handled using CoMOGA alone, eliminating the need for additional variables. Furthermore, we analyze the convergence of the proposed method from a Pareto-optimal perspective and show that the proposed method converges to a local Pareto-optimal policy.

In order to evaluate the proposed method, experiments are conducted across diverse environments, including multi-objective tasks with and without constraints. We use well-known MORL metrics, namely hypervolume and sparsity (Xu et al., 2020), to gauge performance. The experimental results demonstrate that the proposed method achieves the best hypervolume and sparsity in the majority of tasks while successfully adhering to the constraints in all tasks. Finally, our contributions are summarized as follows:

- We propose a scale-invariant CMORL algorithm that does not require additional optimization variables.
- We theoretically show that the proposed method keeps satisfying constraints and converges to a local Pareto optimum under mild assumptions.
- The proposed method outperforms baseline methods in terms of MORL metrics and constraint satisfaction

in various experiments.

2. Related Work

Multi-Objective RL. MORL aims to find a set of Pareto-optimal policies that are not dominated by each other. Given that Pareto-optimal policies can be obtained with appropriate reward scalarization (Hayes et al., 2022), many MORL algorithms utilize scalarization techniques. Based on linear scalarization, Yang et al. (2019) introduced a new Bellman operator for MORL algorithms, which estimates a target Q value for a given preference by combining Q values from other preferences. Basaklar et al. (2023) presented a similar Bellman operator and extended it to an actor-critic framework to enable its application in continuous action spaces. For the continuous action spaces, Lu et al. (2023) proposed a SAC-based MORL algorithm, theoretically demonstrating that elements of the Pareto-optimal policy set can be achieved through linear scalarization. Not only the linear scalarization, Van Moffaert et al. (2013) proposed a non-linear scalarization method, called *Chebyshev* scalarization, which can cover a non-convex policy set. To further improve performance, the evolution strategy (ES) can be applied as done in multi-objective optimization criteria (Deb et al., 2000). Chen et al. (2020) and Xu et al. (2020) proposed methods that repetitively update a policy for each population using linear scalarization and produce a new generation of policy parameters. However, such scalarization exhibits sensitivity to the scale of objectives. To tackle this issue, Abdolmaleki et al. (2020) introduce a scale-invariant algorithm termed *MOMPO*, which does not use scalarization like our proposed approach. This is further extended to a CMORL algorithm (Huang et al., 2022). MOMPO finds a set of policies in the distribution space instead of the reward space by heuristically calculating non-parametric policies. Due to the heuristics, MOMPO does not ensure convergence to a local Pareto-optimal policy, but our method is not only scale-invariant but also guarantees convergence.

Constrained RL. Constrained RL is developed to explicitly consider safety or constraints in RL. Based on the approach to handling constraints, constrained RL algorithms can be categorized into three types: primal-dual methods, primal methods, and dual methods. The primal-dual methods, also called Lagrangian methods, are designed to address Lagrange dual problems. Ding et al. (2022) introduced a natural policy gradient-based primal-dual method and demonstrated its convergence to an optimal policy at a specified convergence rate. Another primal-dual method, proposed by Bai et al. (2022), ensures that a trained policy results in zero constraint violations during evaluation. While these methods are straightforward to implement and can be integrated with standard RL algorithms, the training process can be unstable due to additional optimization variables (La-

grange multipliers) (Stooke et al., 2020). In contrast to the primal-dual method, the primal method addresses the constrained RL problem directly, so no additional optimization variables are required. Achiam et al. (2017) introduced a trust region-based primal method. This approach linearly approximates a constraint within a trust region and updates the policy through a line search. Xu et al. (2021) presented a natural policy gradient-based algorithm and demonstrated its convergence rate towards an optimal policy. In multi-constrained settings, Kim et al. (2023) proposed a primal method named *SDAC* to handle infeasible starting cases. Lastly, dual methods aim to resolve the constrained RL problem within the state distribution space rather than the policy space, and Lee et al. (2022) use this approach. However, because the dual methods still need to use Lagrange multipliers to handle constraints, we have decided to develop a CMORL algorithm based on the primal methods.

3. Background

Constrained Multi-Objective MDP. We define a constrained multi-objective Markov decision process (CMOMDP) as a tuple represented by $\langle S, A, \mathcal{P}, R, C, \rho, \gamma \rangle$, where S is a state space, A is an action space, $\mathcal{P} : S \times A \times S \mapsto [0, 1]$ is a transition model, $R : S \times A \times S \mapsto \mathbb{R}^N$ is a vectorized reward function, $C : S \times A \times S \mapsto \mathbb{R}^M$ is a vectorized cost function, ρ is an initial state distribution, and γ is a discount factor. The reward function R has an upper bound R_{\max} , satisfying $R_{\max} \geq |R_i(\cdot, \cdot, \cdot)| \forall i$. In the CMOMDP setting, a policy $\pi(\cdot|s) \in \Pi$ can be defined as a state-conditional action distribution. The objective function of the i th reward is defined as:

$$J_{R_i}(\pi) := \mathbb{E} \left[\sum_{t=0}^{\infty} \gamma^t R_i(s_t, a_t, s_{t+1}) \right], \quad (1)$$

where $s_0 \sim \rho$, $a_t \sim \pi(\cdot|s_t)$, and $s_{t+1} \sim \mathcal{P}(\cdot|s_t, a_t) \forall t$. We also define the constraint function $J_{C_k}(\pi)$ by replacing the reward with the cost function. A constrained multi-objective RL (CMORL) problem is defined as:

$$\begin{aligned} & \text{maximize}_{\pi} J_{R_i}(\pi) \forall i \in \{1, \dots, N\} \\ & \text{s.t. } J_{C_k}(\pi) \leq d_k \forall k \in \{1, \dots, M\}, \end{aligned} \quad (2)$$

where d_k is the threshold of the k th constraint. Here, it is difficult to determine which policy is optimal when there are multiple objectives. To address this, we instead define a set of optimal policies using the following notion, called *constrained dominance* (Miettinen, 1999):

Definition 3.1 (Constrained Dominance). Given two policies $\pi_1, \pi_2 \in \{\pi \in \Pi | J_{C_k}(\pi) \leq d_k \forall k\}$, π_1 is dominated by π_2 if $J_{R_i}(\pi_1) \leq J_{R_i}(\pi_2) \forall i \in \{1, \dots, N\}$.

A policy π which is not dominated by any policy is called a *constrained-Pareto (CP) optimal* policy, and the set of all CP optimal policies is called *constrained-Pareto (CP) front*

(Miettinen, 1999). In conclusion, we can say that CMORL aims to find a subset of the CP front.

Preference. In order to express a subset of the CP front, many existing MORL works (Xu et al., 2020; Alegre et al., 2023) introduce a preference space, defined as: $\Omega := \{\omega \in \mathbb{R}^N | \omega_i \geq 0, \|\omega\|_{\infty} = 1\}$,¹ where a preference $\omega \in \Omega$ serves to specify the relative significance of each objective. We denote the set of indices representing the maximum preference values as $I_{\omega} := \{i | \omega_i = 1\}$. Subsequently, a specific subset of the Pareto front can be characterized by a function mapping from the preference space to the policy space. We denote this function as a *universal policy* $\pi(\cdot|s, \omega)$, which is characterized as an action distribution contingent upon both the state and preference. As a result, our goal is to train the universal policy to cover the CP front as extensively as possible.

Linear Scalarization. Linear scalarization (LS) is a general approach to deal with the multi-objective optimization problem (2), and it is achieved by solving the following problem given a preference ω :

$$\text{maximize}_{\pi} \sum_{i=1}^N \omega_i J_{R_i}(\pi) \text{ s.t. } J_{C_k}(\pi) \leq d_k \forall k. \quad (3)$$

The above can be addressed by converting it into a Lagrange dual problem and then concurrently updating the policy and Lagrange multipliers. An actor-critic-based MORL algorithm such as CAPQL (Lu et al., 2023) and PD-MORL (Basaklar et al., 2023) can be employed for the policy update. For more details, please refer to Appendix B.3.1. However, LS is sensitive to the scale of objectives. Intuitively, increasing the scale of the i th reward has the same effect as increasing ω_i . Because of this, even if ω is the same, it may be mapped to a different policy depending on how the rewards are scaled. If training is conducted with an increased scale for the i th reward, the trained policy set may focus on maximizing the i th objective. As a result, LS is hard to guarantee that the policy set is evenly distributed in the reward space, which increases the likelihood that there is no user-preferred policy in the trained policy set. Therefore, we develop a scale-invariant CMORL algorithm without LS.

4. Proposed Method

In this section, our discussion will unfold in three parts: 1) introduce a method to calculate policy gradients for a single preference, 2) present a method for training a universal policy that encompasses a spectrum of preferences, and 3) conclude the section with an analysis of the convergence properties of the proposed method.

¹It is common to define the preference space using the norm $\|\omega\|_1$, but for convenience, we employ $\|\omega\|_{\infty}$. Additionally, an one-to-one conversion exists between these definitions.

4.1. Constrained Multi-Objective Gradient Aggregator

We propose a gradient aggregation method called constrained multi-objective gradient aggregator (CoMOGA), which calculates a policy gradient to improve the objectives and comply with the constraints utilizing their respective gradients. The fundamental concept behind the proposed method is to transform the objectives into constraints to circumvent the difficulty in directly handling multiple objectives. For this transformation, we only use the directional component of the objective’s gradient, making the method invariant to the objective scales. We first introduce the transformation process in a simplified problem and extend it to the original CMORL problem. Then, the obtained constrained optimization problem is solved within a local region of the parameter space through linear approximation so as to avoid the need for additional optimization variables.

First, we parameterize a policy and define gradients of the objective and constraint functions, as well as a local region in the parameter space. By representing the policy as π_θ with a parameter $\theta \in \Theta$, the gradients of the objective and constraint functions in (2) are expressed as follows:

$$g_i := \nabla_\theta J_{R_i}(\pi_\theta), \quad b_k := \nabla_\theta J_{C_k}(\pi_\theta). \quad (4)$$

We will denote the objectives as $J_{R_i}(\theta)$ and the constraints as $J_{C_k}(\theta)$ for brevity. The local region is then defined using a positive definite matrix H for a general expression, as follows: $\|\Delta\theta\|_H \leq \epsilon$, where $\|x\|_H := \sqrt{x^T H x}$, the local region size ϵ is a hyperparameter, and H can be the identity matrix or the Hessian of the KL divergence between the current and updated policies, as in TRPO (Schulman et al., 2015).

Next, we introduce the process of converting objectives into constraints. We first present the transformation process in a simplified problem where only the i th objective exists and then extend it to the original problem. The problem of maximizing the i th objective within the local region is expressed as follows:

$$\max_{g \in \Theta} J_{R_i}(\theta_{\text{old}} + g) \quad \text{s.t.} \quad \|g\|_H \leq \epsilon. \quad (5)$$

Assuming that $J_{R_i}(\theta)$ is linear with respect to θ within the local region, the above problem has the same solution as the following problem:

$$\min_{g \in \Theta} \|g\|_H \quad \text{s.t.} \quad e_i \leq J_{R_i}(\theta_{\text{old}} + g) - J_{R_i}(\theta_{\text{old}}), \quad (6)$$

where $e_i := \epsilon \|g_i\|_{H^{-1}}$. It is shown that the solutions to (5) and (6) are identical in Appendix A.1, and this finding confirms that objectives can be converted into constraints in this way. Before extending this process to the original problem (2), we scale e_i in (6), which represents the degree of increase in $J_{R_i}(\theta)$, by the preference value ω_i to reflect a given preference ω . Consequently, the transformed problem

is written as follows:

$$\begin{aligned} \min_g \|g\|_H \quad \text{s.t.} \quad \omega_i e_i \leq J_{R_i}(\theta_{\text{old}} + g) - J_{R_i}(\theta_{\text{old}}) \quad \forall i, \\ J_{C_k}(\theta_{\text{old}} + g) \leq d_k \quad \forall k. \end{aligned} \quad (7)$$

Now, we calculate the policy gradient by solving (7) through approximation. By linearly approximating the objective and constraint functions, (7) becomes a quadratic programming (QP) problem, which can be solved using a QP solver (Goldfarb & Idnani, 1983). However, due to the approximation, there is a risk of violating the constraints during a policy update. In order to handle this issue, we marginally reduce the threshold to $d'_k := d_k - K\epsilon$, where $K \in \mathbb{R}_{\geq 0}$ is a hyperparameter. Additionally, if the constraint values are significantly lower than the thresholds, there is no need to consider those constraints. Therefore, we only consider active constraints, whose indices are defined as $I_{AC}^\epsilon := \{k | d'_k - \epsilon \|b_k\|_{H^{-1}} \leq J_{C_k}(\theta_{\text{old}})\}$. Then, the aggregated gradient can be calculated by solving the following problem using a QP solver:

$$\begin{aligned} \bar{g}_\omega^{\text{ag}} := \operatorname{argmin}_g \|g\|_H \quad \text{s.t.} \quad \omega_i e_i \leq g_i^T g \quad \forall i, \\ b_k^T g + J_{C_k}(\theta_{\text{old}}) \leq d'_k \quad \forall k \in I_{AC}^\epsilon. \end{aligned} \quad (8)$$

For more details on solving (8), see Appendix B.3.2. Since e_i is proportional to the scale of g_i , only the directional component of the gradient g_i remains in the transformed constraints. Due to this, the proposed method is not affected by the scale of objectives. Furthermore, a policy updated using the aggregated gradient with a proper step size can enhance the objectives and satisfy the constraints.

Lemma 4.1. *Assume that the gradients of the objective and constraint functions are L -Lipschitz continuous. If $J_{C_k}(\theta_{\text{old}}) \leq d_k$ for $k \in I_{AC}^\epsilon$, updating the policy parameter with the following step size β ensures $J_{R_i}(\theta_{\text{old}}) \leq J_{R_i}(\theta_{\text{new}})$ for $i \in I_\omega$ and $J_{C_k}(\theta_{\text{new}}) \leq d_k$ for $k \in I_{AC}^\epsilon$:*

$$\begin{aligned} \theta_{\text{new}} = \theta_{\text{old}} + \beta \bar{g}_\omega^{\text{ag}}, \quad \text{where } 0 \leq \beta \leq 1, \\ \beta \leq 2 \|\bar{g}_\omega^{\text{ag}}\|_H / (\alpha L \|\bar{g}_\omega^{\text{ag}}\|_2^2), \end{aligned} \quad (9)$$

$$\alpha := \|\bar{g}_\omega^{\text{ag}}\|_H / \min(K\epsilon, \min_{i \in I_\omega}(e_i)).$$

The proof is provided in Appendix A.2. Lemma 4.1 shows that if the step size satisfies (9), updating a policy with $\bar{g}_\omega^{\text{ag}}$ not only improves the objectives but also consistently keeps the active constraints below the thresholds. We now propose a proper β for stable policy training while meeting the above conditions. From (9), it is observed that β should be reduced when the magnitude of $\bar{g}_\omega^{\text{ag}}$ and α increase. Through this observation, we suggest clipping the policy gradient such that $\bar{g}_\omega^{\text{ag}}$ does not exceed the local region. Similarly, we scale down the policy gradient if α exceeds a specific value, denoted by $G \in \mathbb{R}_{>0}$. Therefore, the final proposed step size is expressed as follows:

$$\begin{aligned} g_\omega^{\text{ag}} := \beta_1 \beta_2 \bar{g}_\omega^{\text{ag}}, \quad \text{where } \beta_1 := \min(1, \epsilon / \|\bar{g}_\omega^{\text{ag}}\|_H), \\ \beta_2 := \min(1, G/\alpha), \end{aligned} \quad (10)$$

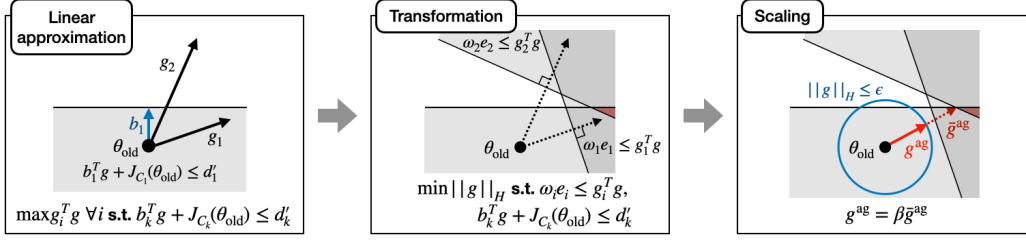


Figure 2: **Process of CoMOGA.** We visualize the process in the parameter space, and the gray areas represent constraints. **(Linear approximation)** CoMOGA linearly approximates the original CMORL problem in (2). The gradients of the objective and constraint functions are visualized as black and blue arrows, respectively. **(Transformation)** The objectives are converted to constraints as described in (8). The intersection of all constraints is shown as the red area. **(Scaling)** The solution of the transformed problem, \bar{g}^{ag} , is scaled to ensure increasing the objectives and continuously satisfying the constraints.

where G is a hyperparameter. Then, we can show that the updated policy using the above gradient can improve the objectives and maintain constraint satisfaction.

Theorem 4.2. *Assume that the gradients of the objectives and constraints are L -Lipschitz continuous. If $J_{C_k}(\theta_{\text{old}}) \leq d_k \forall k$, there exists $\epsilon > 0$ such that the updated policy parameter using CoMOGA, $\theta_{\text{new}} = \theta_{\text{old}} + g_{\omega}^{\text{ag}}$, improves $J_{R_i}(\theta)$ for $i \in I_{\omega}$ and satisfies $J_{C_k}(\theta_{\text{new}}) \leq d_k \forall k$.*

The proof is provided in Appendix A.2 and shows that a larger G or a smaller K necessitates a smaller ϵ . To better understand the role of each hyperparameter, ϵ , K , and G , please refer to the results of ablation studies in Appendix C. Finally, the process of CoMOGA is illustrated in Figure 2.

4.2. Universal Policy Update

We have introduced a gradient aggregation method named *CoMOGA* for updating a policy for a given single preference. This section presents a method for updating a universal policy that can cover the entire preference space. To achieve this, we randomly select P preferences, $\{\omega^p\}_{p=1}^P$, from the preference space and calculate the corresponding aggregated gradients for each preference. Using these P gradients, we can formulate P intermediate policies, defined as $\bar{\pi}_p := \pi_{\theta_p}$, where $\theta_p := \theta_{\text{old}} + g_{\omega^p}^{\text{ag}}$. Now, we need to find a parameter of the universal policy such that $\pi_{\theta_{\text{new}}}(\cdot, \omega^p) = \bar{\pi}_p(\cdot, \omega^p)$ for $\forall p = 1, 2, \dots, P$. To this end, the final step involves updating the parameter to minimize the KL divergence across all the intermediate policies as follows:

$$\min_{\theta} \sum_{p=1}^P \mathbb{E}_{s \sim \mathcal{D}} [D_{\text{KL}}(\bar{\pi}_p(\cdot|s, \omega^p) || \pi_{\theta}(\cdot|s, \omega^p))], \quad (11)$$

where \mathcal{D} is a replay buffer. By minimizing the above loss, we can combine policies for each preference into a single universal policy.

4.3. Convergence Analysis

This section analyzes whether the proposed method converges and, if so, where it converges. Our analysis is grounded on the following three assumptions:

Assumption 4.3. **1)** The gradients of the objectives and constraints are L -Lipschitz continuous, **2)** the constraints are convex, **3)** and $\{\theta | J_{C_k}(\theta) < d_k', \forall k\} \neq \emptyset$.

The first assumption is common in multi-objective approaches for multi-task learning (Liu et al., 2021; Navon et al., 2022). The last two assumptions are used in multi-constrained RL works (Kim et al., 2023) and are intended to ensure the existence of a solution that satisfies the constraints, which can be viewed as the Slater condition (Boyd & Vandenberghe, 2004). Before proceeding further, we define a concept termed *constrained-Pareto (CP) stationarity*.

Definition 4.4 (Constrained-Pareto Stationarity). Given a feasible policy parameter $\theta \in \{\theta | J_{C_k}(\theta) \leq d_k \forall k\}$, the policy π_{θ} is CP stationary if there exist $\lambda \in \mathbb{R}_{\geq 0}^N$ and $\nu \in \mathbb{R}_{\geq 0}^M$ that satisfy the following:

$$\sum_{i=1}^N \lambda_i \nabla_{\theta} J_{R_i}(\theta) = \sum_{k=1}^M \nu_k \nabla_{\theta} J_{C_k}(\theta), \quad (12)$$

where $\sum_i \lambda_i = 1$ and $\nu_k = 0$ for $k \in \{k | J_{C_k}(\theta) < d_k\}$.

We add constraint-related terms to the definition of the Pareto stationarity (Désidéri, 2012). We can then show that CP stationarity is a necessary condition for CP optimality.

Theorem 4.5. *If a policy π_{θ} is CP optimal, the policy is CP stationary. If the objectives are concave, the opposite also holds true.*

The proof can be found in Appendix A.2. Through Theorem 4.5, a CP stationary policy can be viewed as a local CP optimal policy. Additionally, we further define the following relaxed stationarity condition.

Definition 4.6 (ϵ -CP Stationarity). For a policy parameter $\theta \in \{\theta | J_{C_k}(\theta) \leq d_k \forall k\}$, the policy is ϵ -CP stationary if there exist $\lambda \in \mathbb{R}_{\geq 0}^N$ and $\nu \in \mathbb{R}_{\geq 0}^M$ satisfying (12), $\sum_i \lambda_i = 1$, and $\nu_k = 0$ for $k \notin I_{AC}^{\epsilon}$, which is defined in (8).

The definition is the same as CP stationarity except the condition for $\nu_k = 0$. When $\epsilon = 0$, ϵ -CP stationarity is identical to CP stationarity, so the CP stationary set is a subset of the

ϵ -CP stationary set. We can now show that training a policy using CoMOGA converges to a ϵ -CP stationary policy.

Theorem 4.7. *By updating a policy using CoMOGA, the policy converges to a ϵ -CP stationary policy. Furthermore, if there is no solution to (8), the current policy is ϵ -CP stationary.*

The proof of Theorem 4.7 is presented in Appendix A.2. For a simple explanation of the proof, the proposed method monotonically improves the objectives for $i \in I_\omega$. Then, the updated policy will reach some point where either the objectives do not increase or a solution for (8) does not exist. At this point, we have shown the existence of λ and ν satisfying the conditions of Definition 4.6.

5. Practical Implementation

This section covers practical considerations related to algorithm implementation, such as calculating the gradients of the objectives and handling feasibility issues.

Gradient Calculation. To perform CoMOGA and the universal policy update, we need to calculate the gradient of the objective and constraint functions. To do that, we estimate the objectives and constraints using reward and cost critics $V_{R,\psi_R}^\pi, V_{C,\psi_C}^\pi$, where ψ_R and ψ_C are the critic network parameters, for a given preference ω as follows:

$$\begin{aligned} J_{R_i}(\theta) &\approx \mathbb{E}_{s \sim \mathcal{D}} [V_{R_i,\psi_R}^\pi(s, a, \omega) | a \sim \pi_\theta(\cdot | s, \omega)], \\ J_{C_k}(\theta) &\approx \mathbb{E}_{s \sim \mathcal{D}} [V_{C_k,\psi_C}^\pi(s, a, \omega) | a \sim \pi_\theta(\cdot | s, \omega)]. \end{aligned} \quad (13)$$

Then, we can compute the gradients using the critic networks as done in the SAC algorithm (Haarnoja et al., 2018).

Feasibility Handling. CoMOGA ensures that if the current policy satisfies the constraints, the updated policy also satisfies them. However, if the current policy does not satisfy the constraints, the policy should be recovered to the feasible region, $\{\theta | J_{C_k}(\theta) \leq d_k \forall k\}$. To handle this issue, we utilize the gradient integration method (GIM) proposed by Kim et al. (2023), which calculates a gradient toward the feasible region under multiple constraint settings. Finally, the proposed method is summarized in Algorithm 1.

6. Experiments

This section evaluates the proposed method and baselines across various tasks with and without constraints. First, we explain how methods are evaluated on overall tasks and then present the CMORL baselines. Subsequently, each task is described, and the results are analyzed. Finally, we conclude this section with ablation studies of the proposed method.

Algorithm 1 Policy Update Rule Using CoMOGA

Input: Policy parameter θ , reward critic parameter ψ_R , cost critic parameter ψ_C , replay buffer \mathcal{D} .
for epochs = 1 **to** E **do**
 for rollouts = 1 **to** L **do**
 Sample a preference $\omega \sim \Omega$.
 Collect a trajectory $\tau = \{(s_t, a_t, r_t, c_t, s_{t+1})\}_{t=1}^T$ by using $\pi_\theta(\cdot | \cdot, \omega)$ and store τ in \mathcal{D} .
 end for
 Update reward and cost critic networks with \mathcal{D} .
 for $p = 1$ **to** P **do**
 Sample $\omega^p \sim \Omega$, and estimate the objectives and constraints using Equation (13).
 if Constraints are satisfied **then**
 Calculate the aggregated gradient $g_{\omega^p}^{\text{ag}}$ using Equation (8), and set $\theta_p = \theta + g_{\omega^p}^{\text{ag}}$.
 else
 Calculate the recovery gradient g_r using GIM as described in Section 5, and set $\theta_p = \theta + g_r$.
 end if
 Store an intermediate policy $\bar{\pi}_p = \pi_{\theta_p}$.
 end for
 Update the universal policy using Equation (11).
end for

6.1. Evaluation Metrics and Baselines

Once the universal policy is trained, an estimated CP front, denoted as $P \subset \mathbb{R}^N$, can be obtained by calculating the objective values $(J_{R_1}(\pi), \dots, J_{R_N}(\pi))$ for a range of preferences. Given that CMORL aims to approximate the ground truth CP front, it is essential to assess how close the estimated CP front is to the ground truth, and it can be realized by measuring the coverage and density of the estimated front. To this end, we use the *hypervolume* (HV) for coverage measurement and *sparsity* (SP) for density estimation, which are commonly used in many MORL algorithms (Xu et al., 2020; Basaklar et al., 2023). Given an estimated CP front $P \subset \mathbb{R}^N$ and a reference point $r \in \mathbb{R}^N$, the hypervolume (HV) is defined as follows (Zitzler & Thiele, 1999):

$$\text{HV}(P, r) := \int_{\mathbb{R}^N} \mathbf{1}_{Q(P,r)}(z) dz, \quad (14)$$

where $Q(P, r) := \{z | \exists p \in P \text{ s.t. } r \preceq z \preceq p\}$. HV is then the volume of the area surrounding the reference point and the estimated CP front. For a detailed explanation of this metric, including a visual description and how the reference point is set, please refer to Appendix B.2. Sparsity (SP), on the other hand, measures how uniformly the estimated CP fronts are distributed and is defined as the average of the squared distances between elements (Xu et al., 2020):

$$\text{SP}(P) := \frac{1}{|P| - 1} \sum_{j=1}^N \sum_{i=1}^{|P|-1} (\tilde{P}_j(i) - \tilde{P}_j(i+1))^2, \quad (15)$$

where $\tilde{P}_j := \text{Sort}(\{p_j | \forall p \in P\})$, and $\tilde{P}_j(i)$ is the i th element in \tilde{P}_j . Since a larger value indicates a less dense set, it is preferred to have a small value. However, given that

Table 1: **Results of the Safety Gymnasium tasks.** The hypervolume (HV), sparsity (SP), and constraint values (Con1, Con2) are obtained by averaging results from five random seeds. The thresholds for each constraint are shown after Con1 and Con2, and elements that violate constraints are shown in red. Since the single-agent tasks have only a single constraint, so Con2 does not exist.

	Single-Point-Goal				Single-Car-Goal			
	HV ($\times 10^1$) \uparrow	SP ($\times 10^{-1}$) \downarrow	Con1 (≤ 0.025)	Con2 (≤ 0.025)	HV ($\times 10^1$) \uparrow	SP ($\times 10^{-1}$) \downarrow	Con1 (≤ 0.025)	Con2 (≤ 0.025)
CAPQL	2.347	0.861	0.026	-	0.085	4.472	0.019	-
PD-MORL	2.709	1.255	0.024	-	0.070	3.112	0.027	-
LP3	3.807	4.441	0.035	-	0.701	15.519	0.037	-
CoMOGA (Ours)	3.628	0.511	0.022	-	1.057	0.558	0.024	-
	Multi-Point-Goal				Multi-Car-Goal			
CAPQL	17.089	1.445	0.019	0.023	51.401	1.604	0.016	0.022
PD-MORL	0.000	9.878	0.007	0.013	0.000	6.187	0.036	0.052
LP3	31.856	x	0.032	0.047	9.554	16.475	0.033	0.043
CoMOGA (Ours)	38.646	2.010	0.022	0.019	65.895	1.115	0.022	0.017

the cardinality of the set P is constant, a larger HV typically corresponds to a greater SP. To remove this inherent correlation, we propose the following normalized version:

$$\overline{SP}(P) := \frac{1}{|P| - 1} \sum_{j=1}^N \sum_{i=1}^{|P|-1} \left(\frac{\tilde{P}_j(i) - \tilde{P}_j(i+1)}{\max_k \tilde{P}_j(k) - \min_k \tilde{P}_j(k)} \right)^2, \tag{16}$$

where the elements of the sorted array \tilde{P}_j are normalized with respect to their maximum and minimum values. By using the normalized sparsity, we can eliminate the correlation with HV while preserving the ability to measure sparsity.

For comparison with the proposed method, we first employ *LP3* (Huang et al., 2022), a CMORL algorithm, as a baseline. This method extends the scale-invariant MORL algorithm, *MOMPO* (Abdolmaleki et al., 2020), to CMORL by handling constraints in a similar way to the Lagrangian method. Subsequently, we utilize state-of-the-art actor-critic-based MORL algorithms, *PD-MORL* (Basaklar et al., 2023) and *CAPQL* (Lu et al., 2023), which are based on linear scalarization. They are respectively implemented based on the TD3 (Fujimoto et al., 2018) and SAC (Haarnoja et al., 2018) algorithms. We extend them to CMORL algorithms by handling constraints using the Lagrangian method, like LP3, and please see Appendix B.3.1 for implementation details.

6.2. Safety Gymnasium

We utilize single-agent and multi-agent goal tasks from the constrained RL environment, Safety Gymnasium (Ji et al., 2023). These tasks require navigating robots to designated goals while avoiding obstacles. The single-agent goal task has two objectives: 1) reaching goals as many times as possible within a time limit and 2) maximizing energy efficiency, along with a single constraint to avoid collisions with obstacles. Conversely, the multi-agent goal task involves two agents and two goals, requiring control of both agents to reach goals competitively. It encompasses two objectives, maximizing goal achievement for each agent, and two constraints to avoid obstacle collisions for each robot. Various types of robots are available for these tasks, among which

point and car robots are used. For details on the tasks and hyperparameter settings, please refer to Appendix B.

The results are presented in Table 1, and the visualization of the estimated Pareto fronts can be found in Appendix C. The proposed method shows superior performance, achieving the highest HV and the lowest SP in three out of four tasks while satisfying the constraints across all tasks. On the other hand, other baselines violate constraints in at least one task, confirming that the proposed method can handle constraints more stably as it does not need additional optimization variables. LP3 shows the best HV in the Single-Point-Goal but violates the constraint. Moreover, in the Multi-Point-Goal, the SP of LP3 cannot be obtained because the estimated CP front of LP3 contains only one element due to constraint violation, so we leave this item empty in Table 1.

6.3. Legged Robot Locomotion

To evaluate the proposed method in more complex environments, we utilize the locomotion tasks from Kim et al. (2023), where the dimension of the action space is at least ten. The task is to control a quadrupedal or bipedal robot to follow randomly given commands while satisfying three constraints: keeping 1) body balance, 2) CoM height, and 3) pre-defined foot contact timing. Additionally, we have modified the tasks to have two objectives: 1) matching the current velocity with the command and 2) minimizing energy consumption. Please see Appendix B for more details.

We present the results of locomotion tasks in Table 2, and the proposed method shows the best HV and SP while satisfying constraints in all tasks. In these tasks, handling constraints using the Lagrangian method is more challenging since the number of Lagrange multipliers increases due to the multiple constraints. Because of this, PD-MORL and CAPQL show low HV and high SP values. We cannot calculate the SP of PD-MORL in the quadrupedal task for the same reason as in the Multi-Point-Goal task of LP3, so we leave it empty. LP3 shows comparable performance to the proposed method in the quadrupedal task, suggesting that

Table 2: **Results of the locomotion tasks.** The hypervolume (HV), sparsity (SP), and constraint values (Con1, Con2, Con3) are obtained by averaging results from five random seeds. The thresholds for each constraint are shown after Con1, Con2, and Con3, and elements that violate the constraint are shown in red.

	Quadruped					Biped				
	HV ($\times 10^4$) \uparrow	\overline{SP} ($\times 10^{-1}$) \downarrow	Con1 (≤ 0.025)	Con2 (≤ 0.025)	Con3 (≤ 0.4)	HV ($\times 10^4$) \uparrow	\overline{SP} ($\times 10^{-1}$) \downarrow	Con1 (≤ 0.025)	Con2 (≤ 0.025)	Con3 (≤ 0.4)
CAPQL	0.000	7.533	0.023	0.031	0.232	0.000	9.127	0.002	0.001	0.013
PD-MORL	0.000	x	0.067	0.190	0.499	0.000	14.349	0.013	0.004	0.410
LP3	4.637	0.170	0.024	0.009	0.201	0.114	1.991	0.004	0.002	0.356
CoMOGA (Ours)	4.936	0.169	0.015	0.014	0.338	7.067	0.177	0.002	0.002	0.359

Table 3: **Results of the MO-Gymnasium tasks.** HV and SP are obtained by averaging results from five random seeds.

	Half-Cheetah		Hopper		Water-Reservoir		Lunar-Lander	
	HV ($\times 10^5$) \uparrow	\overline{SP} ($\times 10^{-1}$) \downarrow	HV ($\times 10^8$) \uparrow	\overline{SP} ($\times 10^{-1}$) \downarrow	HV ($\times 10^4$) \uparrow	\overline{SP} ($\times 10^{-1}$) \downarrow	HV ($\times 10^8$) \uparrow	\overline{SP} ($\times 10^{-1}$) \downarrow
CAPQL	10.418	1.211	0.152	8.103	1.869	0.688	13.517	0.180
PD-MORL	0.959	2.045	0.064	0.786	2.829	1.022	9.379	3.419
LP3	3.557	0.720	0.000	0.877	1.417	1.615	0.606	9.471
CoMOGA (Ours)	16.903	0.166	17.468	0.492	1.670	0.580	17.365	0.259

LP3 can update policies more stably than other baselines because it updates the policy in the distribution space rather than the reward space.

6.4. Multi-Objective Gymnasium

We conduct experiments in the Multi-Objective (MO) Gymnasium (Alegre et al., 2022), which is a well-known MORL environment, to examine whether the proposed method also performs well on unconstrained MORL tasks. We use tasks with continuous action spaces in the MO Gymnasium, and there are four tasks available: Half-Cheetah, Hopper, Water-Reservoir, and Lunar-Lander. Each task has two, three, two, and four objectives, respectively. For more details, please refer to Appendix B. The results are presented in Table 3, and the proposed method achieves the best HV and SP in three out of the four tasks. These results suggest that the proposed gradient aggregation strategy, which involves transforming objectives into constraints, is also effective in unconstrained multi-objective tasks.

6.5. Invariance to Objective Scales

In this section, we compare the proposed method with the linear scalarization approach in terms of sensitivity to the scale of objectives. To do this, we prepare a linear scalarization (LS) version of CoMOGA, which linearly sums the objectives instead of converting them into constraints. We modify the scale of the energy efficiency objective in the quadrupedal task by providing agents with $10\times$ and $0.1\times$ energy efficiency rewards. The results of the trained universal policy are visualized in Figure 3, and the values of the HV and SP metrics are reported in Appendix C. Observing Figure 3(a), CoMOGA exhibits consistent results between the original and scaled tasks. However, the results of the LS version are concentrated in the upper left for the $10\times$ scaled

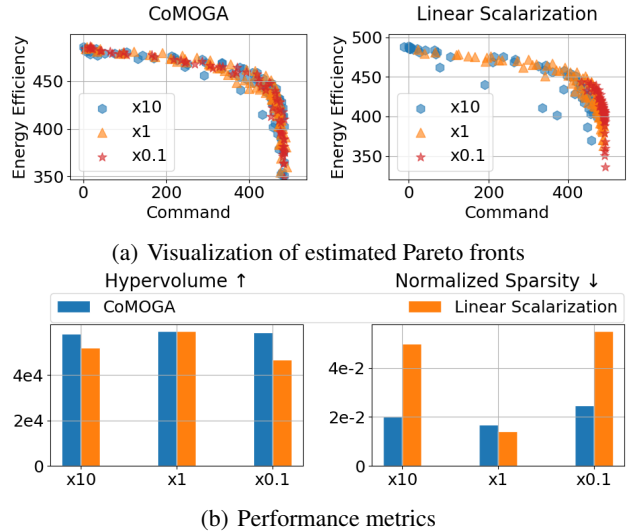


Figure 3: **Comparison CoMOGA with linear scalarization.** The estimated CP fronts obtained from CoMOGA and LS are visualized in (a). For each scaled task, we conduct experiments with five random seeds, plotting the fronts from each seed in the same figure. (b) presents bar graphs showing HV and SP values for each scaled task, with scale details indicated on the x-axis.

task and in the lower right for the $0.1\times$ scaled task, confirming that the LS approach tends to prioritize objectives with large scales. Additionally, Figure 3(b) shows that the metrics of CoMOGA do not vary with the objective scales, but the metrics of LS change significantly. In particular, the SP becomes more than three times larger in the scaled tasks compared to the original task. Through this study, we highlight the sensitivity of LS approaches to the objective scales and indicate that this sensitivity can lead to a degradation in performance.

7. Conclusions

We have introduced a CMORL algorithm, called CoMOGA, to maximize multiple objectives while satisfying constraints. The proposed method is based on a novel transformation process that converts objectives into constraints, which makes the method invariant to the objective scales and capable of handling constraints without additional optimization variables. We theoretically demonstrate that the proposed method converges to a local Pareto optimal policy and show that the proposed method outperforms the baseline methods in terms of CP front coverage and constraint satisfaction through various experiments.

Impact Statements

This paper presents work whose goal is to advance the field of Machine Learning. There are many potential societal consequences of our work, none which we feel must be specifically highlighted here.

References

- Abdolmaleki, A., Huang, S., Hasenclever, L., Neunert, M., Song, F., Zambelli, M., Martins, M., Heess, N., Hadsell, R., and Riedmiller, M. A distributional view on multi-objective policy optimization. In *Proceedings of International Conference on Machine Learning*, pp. 11–22, 2020.
- Achiam, J., Held, D., Tamar, A., and Abbeel, P. Constrained policy optimization. In *Proceedings of International Conference on Machine Learning*, pp. 22–31, 2017.
- Alegre, L. N., Felten, F., Talbi, E.-G., Danoy, G., Nowé, A., Bazzan, A. L. C., and da Silva, B. C. MO-Gym: A library of multi-objective reinforcement learning environments. In *Proceedings of Benelux Conference on Artificial Intelligence BNAIC/Benelearn*, 2022.
- Alegre, L. N., Bazzan, A. L., Roijers, D. M., Nowé, A., and da Silva, B. C. Sample-efficient multi-objective learning via generalized policy improvement prioritization. In *Proceedings of International Conference on Autonomous Agents and Multiagent Systems*, pp. 2003–2012, 2023.
- Bai, Q., Bedi, A. S., Agarwal, M., Koppel, A., and Agarwal, V. Achieving zero constraint violation for constrained reinforcement learning via primal-dual approach. In *Proceedings of the AAAI Conference on Artificial Intelligence*, volume 36, pp. 3682–3689, 2022.
- Basaklar, T., Gumussoy, S., and Ogras, U. PD-MORL: Preference-driven multi-objective reinforcement learning algorithm. In *Proceedings of International Conference on Learning Representations*, 2023.
- Boyd, S. P. and Vandenberghe, L. *Convex optimization*. Cambridge university press, 2004.
- Chen, D., Wang, Y., and Gao, W. Combining a gradient-based method and an evolution strategy for multi-objective reinforcement learning. *Applied Intelligence*, 50:3301–3317, 2020.
- Dabney, W., Rowland, M., Bellemare, M., and Munos, R. Distributional reinforcement learning with quantile regression. *Proceedings of the AAAI Conference on Artificial Intelligence*, 32(1), 2018.
- Deb, K., Agrawal, S., Pratap, A., and Meyarivan, T. A fast elitist non-dominated sorting genetic algorithm for multi-objective optimization: NSGA-II. In *Parallel Problem Solving from Nature PPSN VI*, pp. 849–858, 2000.
- Ding, D., Zhang, K., Duan, J., Başar, T., and Jovanović, M. R. Convergence and sample complexity of natural policy gradient primal-dual methods for constrained mdps. *arXiv preprint arXiv:2206.02346*, 2022.
- Désidéri, J.-A. Multiple-gradient descent algorithm (MGDA) for multiobjective optimization. *Comptes Rendus Mathématique*, 350(5):313–318, 2012.
- Felten, F., Alegre, L. N., Nowe, A., Bazzan, A. L. C., Talbi, E. G., Danoy, G., and da Silva, B. C. A toolkit for reliable benchmarking and research in multi-objective reinforcement learning. In *Proceedings of Conference on Neural Information Processing Systems Datasets and Benchmarks Track*, 2023.
- Fujimoto, S., van Hoof, H., and Meger, D. Addressing function approximation error in actor-critic methods. In *Proceedings of International Conference on Machine Learning*, pp. 1587–1596, 2018.
- Goldfarb, D. and Idnani, A. A numerically stable dual method for solving strictly convex quadratic programs. *Mathematical programming*, 27(1):1–33, 1983.
- Haarnoja, T., Zhou, A., Abbeel, P., and Levine, S. Soft actor-critic: Off-policy maximum entropy deep reinforcement learning with a stochastic actor. In *Proceedings of International Conference on Machine Learning*, pp. 1861–1870, 2018.
- Hayes, C. F., Rădulescu, R., Bargiacchi, E., Källström, J., Macfarlane, M., Reymond, M., Verstraeten, T., Zintgraf, L. M., Dazeley, R., Heintz, F., et al. A practical guide to multi-objective reinforcement learning and planning. *Autonomous Agents and Multi-Agent Systems*, 36(1):26, 2022.
- Huang, S., Abdolmaleki, A., Vezzani, G., Brakel, P., Mankowitz, D. J., Neunert, M., Bohez, S., Tassa, Y.,

- Heess, N., Riedmiller, M., and Hadsell, R. A constrained multi-objective reinforcement learning framework. In *Proceedings of Conference on Robot Learning*, pp. 883–893, 2022.
- Ji, J., Zhang, B., Pan, X., Zhou, J., Dai, J., and Yang, Y. Safety-gymnasium. *GitHub repository*, 2023.
- Kim, D. and Oh, S. Efficient off-policy safe reinforcement learning using trust region conditional value at risk. *IEEE Robotics and Automation Letters*, 7(3):7644–7651, 2022.
- Kim, D., Lee, K., and Oh, S. Trust region-based safe distributional reinforcement learning for multiple constraints. In *Advances in Neural Information Processing Systems*, 2023.
- Kuznetsov, A., Shvechikov, P., Grishin, A., and Vetrov, D. Controlling overestimation bias with truncated mixture of continuous distributional quantile critics. In *Proceedings International Conference on Machine Learning*, pp. 5556–5566, 2020.
- Kyriakis, P. and Deshmukh, J. Pareto policy adaptation. In *Proceedings of International Conference on Learning Representations*, 2022.
- Lee, J., Paduraru, C., Mankowitz, D. J., Heess, N., Precup, D., Kim, K.-E., and Guez, A. COptiDICE: Offline constrained reinforcement learning via stationary distribution correction estimation. In *Proceedings of International Conference on Learning Representations*, 2022.
- Liu, B., Liu, X., Jin, X., Stone, P., and Liu, Q. Conflict-averse gradient descent for multi-task learning. In *Advances in Neural Information Processing Systems*, pp. 18878–18890, 2021.
- Lu, H., Herman, D., and Yu, Y. Multi-objective reinforcement learning: Convexity, stationarity and pareto optimality. In *Proceedings of International Conference on Learning Representations*, 2023.
- Miettinen, K. *Nonlinear multiobjective optimization*, volume 12. Springer Science & Business Media, 1999.
- Navon, A., Shamsian, A., Achituve, I., Maron, H., Kawaguchi, K., Chechik, G., and Fetaya, E. Multi-task learning as a bargaining game. In *Proceedings of International Conference on Machine Learning*, pp. 16428–16446, 2022.
- Roijers, D. M., Vamplew, P., Whiteson, S., and Dazeley, R. A survey of multi-objective sequential decision-making. *Journal of Artificial Intelligence Research*, 48:67–113, 2013.
- Schulman, J., Levine, S., Abbeel, P., Jordan, M., and Moritz, P. Trust region policy optimization. In *Proceedings of International Conference on Machine Learning*, pp. 1889–1897, 2015.
- Stooke, A., Achiam, J., and Abbeel, P. Responsive safety in reinforcement learning by PID lagrangian methods. In *Proceedings of International Conference on Machine Learning*, pp. 9133–9143, 2020.
- Van Moffaert, K., Drugan, M. M., and Nowé, A. Scalarized multi-objective reinforcement learning: Novel design techniques. In *IEEE Symposium on Adaptive Dynamic Programming and Reinforcement Learning (ADPRL)*, pp. 191–199, 2013.
- Xu, J., Tian, Y., Ma, P., Rus, D., Sueda, S., and Matusik, W. Prediction-guided multi-objective reinforcement learning for continuous robot control. In *Proceedings of International Conference on Machine Learning*, pp. 10607–10616, 2020.
- Xu, T., Liang, Y., and Lan, G. CRPO: A new approach for safe reinforcement learning with convergence guarantee. In *Proceedings of International Conference on Machine Learning*, pp. 11480–11491, 2021.
- Yang, R., Sun, X., and Narasimhan, K. A generalized algorithm for multi-objective reinforcement learning and policy adaptation. In *Advances in Neural Information Processing Systems*, 2019.
- Zitzler, E. and Thiele, L. Multiobjective evolutionary algorithms: a comparative case study and the strength pareto approach. *IEEE Transactions on Evolutionary Computation*, 3(4):257–271, 1999.

A. Theoretical Analysis

A.1. Transformation Process

In this section, we prove that the solutions of (5) and (6) are equivalent. Under the linear assumption, we can express the i th objective function as $g_i^T g + J_{R_i}(\theta_{\text{old}})$. Then, (5) can be rewritten as follows:

$$\max_g g_i^T g + J_{R_i}(\theta_{\text{old}}) \quad \text{s.t.} \quad \sqrt{g^T H g} \leq \epsilon. \quad (17)$$

As the strong duality holds, we will find the solution by solving the following Lagrange dual problem:

$$\max_{\lambda \geq 0} \min_g -g_i^T g + \lambda(\sqrt{g^T H g} - \epsilon) =: L(g, \lambda). \quad (18)$$

Then, $g^*(\lambda) = \operatorname{argmin}_g L(g, \lambda) = \frac{1}{2\lambda} H^{-1} g_i$. By substituting $g^*(\lambda)$ to g , we get $\lambda^* = \operatorname{argmax}_{\lambda} L(g^*, \lambda) = \frac{1}{2\epsilon} \sqrt{g_i^T H^{-1} g_i}$. Finally, we obtain the solution, $g^* = g^*(\lambda^*) = \epsilon H^{-1} g_i / \sqrt{g_i^T H^{-1} g_i}$.

Now let us find the solution of (6). Under the linear assumption, we can rewrite (6) as follows:

$$\min_g g^T H g \quad \text{s.t.} \quad e_i \leq g_i^T g. \quad (19)$$

Similar to the above process, the Lagrange dual problem is derived as follows:

$$\max_{\lambda \geq 0} \min_g g^T H g + \lambda(e_i - g_i^T g) =: L(g, \lambda). \quad (20)$$

Then, the solution of the dual problem is obtained as $g^*(\lambda) = \operatorname{argmin}_g L(g, \lambda) = \frac{1}{2} \lambda H^{-1} g_i$. Using $g^*(\lambda)$, we can get the optimal Lagrange multiplier as $\lambda^* = \operatorname{argmax}_{\lambda} L(g^*, \lambda) = 2e_i / (g_i^T H^{-1} g_i) = 2\epsilon / \sqrt{g_i^T H^{-1} g_i}$. Then, the solution is $g^* = g^*(\lambda^*) = \epsilon H^{-1} g_i / \sqrt{g_i^T H^{-1} g_i}$. As a result, the solutions of (5) and (6) are the same as $\epsilon H^{-1} g_i / \sqrt{g_i^T H^{-1} g_i}$.

A.2. Proof of Theorems

Lemma 4.1. *Assume that the gradients of the objective and constraint functions are L -Lipschitz continuous. If $J_{C_k}(\theta_{\text{old}}) \leq d_k$ for $k \in I_{\text{AC}}^\epsilon$, updating the policy parameter with the following step size β ensures $J_{R_i}(\theta_{\text{old}}) \leq J_{R_i}(\theta_{\text{new}})$ for $i \in I_\omega$ and $J_{C_k}(\theta_{\text{new}}) \leq d_k$ for $k \in I_{\text{AC}}^\epsilon$:*

$$\begin{aligned} \theta_{\text{new}} &= \theta_{\text{old}} + \beta \bar{g}_\omega^{\text{ag}}, \text{ where } 0 \leq \beta \leq 1, \\ \beta &\leq 2 \|\bar{g}_\omega^{\text{ag}}\|_H / (\alpha L \|\bar{g}_\omega^{\text{ag}}\|_2^2), \end{aligned} \quad (9)$$

$$\alpha := \|\bar{g}_\omega^{\text{ag}}\|_H / \min(K\epsilon, \min_{i \in I_\omega}(e_i)).$$

Proof. We first check the constraint. Due to the L -Lipschitz continuity assumption,

$$J_{C_k}(\theta_{\text{old}} + \beta \bar{g}_\omega^{\text{ag}}) - J_{C_k}(\theta_{\text{old}}) \leq \beta b_k^T \bar{g}_\omega^{\text{ag}} + \frac{L}{2} \beta^2 \|\bar{g}_\omega^{\text{ag}}\|_2^2. \quad (21)$$

From Equation (8), $b_k^T \bar{g}_\omega^{\text{ag}} \leq d_k - K\epsilon - J_{C_k}(\theta_{\text{old}})$ for $k \in I_{\text{AC}}^\epsilon$. Reordering the above inequality,

$$J_{C_k}(\theta_{\text{old}} + \beta \bar{g}_\omega^{\text{ag}}) - d_k \leq (1 - \beta)(J_{C_k}(\theta_{\text{old}}) - d_k) + \beta \left(\frac{L}{2} \beta \|\bar{g}_\omega^{\text{ag}}\|_2^2 - K\epsilon \right) \leq 0, \quad (22)$$

since $0 \leq \beta \leq 1$ and $\beta \leq 2K\epsilon / (L \|\bar{g}_\omega^{\text{ag}}\|_2^2)$. Thus, the constraint is also satisfied at θ_{new} . Subsequently, we check the objective for $i \in I_\omega$. Using the L -Lipschitz continuity property and (8),

$$J_{R_i}(\theta_{\text{old}} + \beta \bar{g}_\omega^{\text{ag}}) - J_{R_i}(\theta_{\text{old}}) \geq \beta g_i^T \bar{g}_\omega^{\text{ag}} - \frac{L}{2} \beta^2 \|\bar{g}_\omega^{\text{ag}}\|_2^2 \geq \beta \left(e_i - \frac{L}{2} \beta \|\bar{g}_\omega^{\text{ag}}\|_2^2 \right). \quad (23)$$

Since $\beta \leq 2 \|\bar{g}_\omega^{\text{ag}}\|_H / (\alpha L \|\bar{g}_\omega^{\text{ag}}\|_2^2) \leq 2e_i / (L \|\bar{g}_\omega^{\text{ag}}\|_2^2)$,

$$J_{R_i}(\theta_{\text{old}} + \beta \bar{g}_\omega^{\text{ag}}) - J_{R_i}(\theta_{\text{old}}) \geq 0. \quad (24)$$

As a result, updating the policy parameters to θ_{new} will increase the objective for $i \in I_\omega$. \square

Theorem 4.2. Assume that the gradients of the objectives and constraints are L -Lipschitz continuous. If $J_{C_k}(\theta_{\text{old}}) \leq d_k \forall k$, there exists $\epsilon > 0$ such that the updated policy parameter using CoMOGA, $\theta_{\text{new}} = \theta_{\text{old}} + g_{\omega}^{\text{ag}}$, improves $J_{R_i}(\theta)$ for $i \in I_{\omega}$ and satisfies $J_{C_k}(\theta_{\text{new}}) \leq d_k \forall k$.

Proof. Since $g_{\omega}^{\text{ag}} = \beta_1 \beta_2 \bar{g}_{\omega}^{\text{ag}}$, where $\beta_1 = \min(1, \epsilon / \|\bar{g}_{\omega}^{\text{ag}}\|_H)$ and $\beta_2 := \min(1, G/\alpha)$, we only need to show that the step size $\beta = \beta_1 \beta_2$ satisfies the condition of Lemma 4.1 and that $J_{C_k}(\theta_{\text{new}}) \leq d_k$ for $\forall k$. There are two cases regarding α : 1) $\alpha \leq G$ and 2) $\alpha > G$. For the first case $\alpha \leq G$, $\beta = \beta_1$ since $\beta_2 = 1$. Since $0 \leq \beta_1 \leq 1$, it is obvious that $0 \leq \beta \leq 1$. Thus, we only need to check $1 \leq 2\|\bar{g}_{\omega}^{\text{ag}}\|_H / (\alpha\beta L \|\bar{g}_{\omega}^{\text{ag}}\|_2^2)$. Since the matrix H is positive definite, there exist $h > 0$ such that $h\|x\|_2 \leq \|x\|_H$. Then, the following inequality holds:

$$\frac{2\|\bar{g}_{\omega}^{\text{ag}}\|_H}{\alpha L \beta \|\bar{g}_{\omega}^{\text{ag}}\|_2^2} \geq \frac{2h^2}{\alpha L \beta_1 \|\bar{g}_{\omega}^{\text{ag}}\|_H} \geq \frac{2h^2}{\alpha L \epsilon} \geq \frac{2h^2}{GL\epsilon}. \quad (25)$$

Thus, if $\epsilon \leq 2h^2/GL$, the step size satisfies Lemma 4.1. For the second case $\alpha > G$, $\beta = G\beta_1/\alpha$. Similar to the first case, the following inequality holds:

$$\frac{2\|\bar{g}_{\omega}^{\text{ag}}\|_H}{\alpha L \beta \|\bar{g}_{\omega}^{\text{ag}}\|_2^2} \geq \frac{2h^2}{GL\beta_1 \|\bar{g}_{\omega}^{\text{ag}}\|_H} \geq \frac{2h^2}{GL\epsilon}. \quad (26)$$

Therefore, if $\epsilon \leq 2h^2/GL$, the step size condition for Lemma 4.1 is satisfied.

Second, we have to check that $J_{C_k}(\theta_{\text{new}}) \leq d_k$ for $k \notin I_{\text{AC}}^{\epsilon}$. Since $k \notin I_{\text{AC}}^{\epsilon}$, $J_{C_k}(\theta_{\text{old}}) < d_k - \epsilon(K + \sqrt{b_k^T H^{-1} b_k})$. Additionally, from the result of Appendix A.1, we can get the maximum of $b_k^T g$ in the local region by substituting the optimal g^* into $b_k^T g$, which results in $\epsilon \sqrt{b_k^T H^{-1} b_k}$. This means $b_k^T g_{\omega}^{\text{ag}} \leq \epsilon \sqrt{b_k^T H^{-1} b_k}$, since g_{ω}^{ag} is within the local region. Using the above facts and the L -Lipschitz continuity assumption,

$$\begin{aligned} J_{C_k}(\theta_{\text{old}} + \beta_1 \beta_2 \bar{g}_{\omega}^{\text{ag}}) &\leq \beta_1 \beta_2 b_k^T \bar{g}_{\omega}^{\text{ag}} + \frac{L}{2} \beta_1^2 \beta_2^2 \|\bar{g}_{\omega}^{\text{ag}}\|_2^2 + J_{C_k}(\theta_{\text{old}}) \\ &\leq \beta b_k^T \bar{g}_{\omega}^{\text{ag}} + \frac{L}{2} \epsilon^2 \|\bar{g}_{\omega}^{\text{ag}}\|_2^2 / \|\bar{g}_{\omega}^{\text{ag}}\|_H^2 + J_{C_k}(\theta_{\text{old}}) \\ &\leq \beta b_k^T \bar{g}_{\omega}^{\text{ag}} + \frac{L}{2h^2} \epsilon^2 + J_{C_k}(\theta_{\text{old}}) \\ &\leq \epsilon \sqrt{b_k^T H^{-1} b_k} + \frac{L}{2h^2} \epsilon^2 + J_{C_k}(\theta_{\text{old}}) \leq \frac{L}{2h^2} \epsilon^2 - K\epsilon + d_k. \end{aligned} \quad (27)$$

Here, if $\epsilon \leq (2Kh^2)/L$, $J_{C_k}(\theta_{\text{new}}) \leq d_k$. As a result, if $\epsilon \leq 2h^2 \min(K, 1/G)/L$, CoMOGA improves the objectives for $i \in I_{\omega}$ and satisfies $J_{C_k}(\theta_{\text{new}}) \leq d_k$ for $\forall k$. \square

Theorem 4.5. If a policy $\pi_{\bar{\theta}}$ is CP optimal, the policy is CP stationary. If the objectives are concave, the opposite also holds true.

Proof. Let a policy $\pi_{\bar{\theta}}$ is constrained-Pareto optimal. Then the following equation holds:

$$\bar{\theta} = \operatorname{argmin}_{\theta} -J_{R_1}(\theta) \text{ s.t. } J_{R_i}(\bar{\theta}) \leq J_{R_i}(\theta) \forall i \geq 2, J_{C_k}(\bar{\theta}) \leq d_k \forall k.$$

Since the gradients of the objective and constraint functions are continuous, we can get the following by linear approximation at $\theta = \bar{\theta}$:

$$\mathbf{0} = \operatorname{argmin}_d -\nabla J_{R_1}(\bar{\theta})^T d \text{ s.t. } 0 \leq \nabla J_{R_i}(\bar{\theta})^T d \forall i \geq 2, J_{C_k}(\bar{\theta}) + \nabla J_{C_k}(\bar{\theta})^T d \leq d_k \forall k. \quad (28)$$

The dual problem is as follows:

$$\max_{\lambda \geq 0, \nu \geq 0} L(\lambda, \nu) := \min_d -\nabla J_{R_1}(\bar{\theta})^T d - \sum_{i=2}^N \lambda_i J_{R_i}(\bar{\theta})^T d + \sum_{k=1}^M \nu_k (J_{C_k}(\bar{\theta}) - d_k + \nabla J_{C_k}(\bar{\theta})^T d).$$

Since linear programming problems hold strong duality, the stationarity of the KKT condition is satisfied at the optimal dual variables λ^* , ν^* , and $d = \mathbf{0}$ as follows:

$$-\nabla J_{R_1}(\bar{\theta}) - \sum_{i=2}^N \lambda_i^* J_{R_i}(\bar{\theta}) + \sum_{k=1}^M \nu_k^* \nabla J_{C_k}(\bar{\theta}) = \mathbf{0}.$$

Also, by the complementary slackness of the KKT condition, $\nu_k^* = 0$ for $J_{C_k}(\bar{\theta}) < d_k$. By setting $\bar{\lambda}_1 = 1/(1 + \sum_{i=2}^N \lambda_i^*)$, $\bar{\lambda}_{i \geq 2} = \lambda_i^*/(1 + \sum_{i=2}^N \lambda_i^*)$, and $\bar{\nu}_k = \nu_k^*/(1 + \sum_{i=2}^N \lambda_i^*)$, the above equation can be rewritten as follows:

$$\sum_{i=1}^N \bar{\lambda}_i \nabla J_{R_i}(\bar{\theta}) = \sum_{k=1}^M \bar{\nu}_k \nabla J_{C_k}(\bar{\theta}), \quad (29)$$

where $\sum_i \bar{\lambda}_i = 1$, $\bar{\nu}_k = 0$ for $J_{C_k}(\bar{\theta}) < d_k$. Therefore, the policy $\pi_{\bar{\theta}}$ is constrained-Pareto stationary.

We now investigate the proposition that a policy $\pi_{\bar{\theta}}$ is constrained-Pareto optimal if it is constrained-Pareto stationary, under the assumption that the objectives are concave. Since $\pi_{\bar{\theta}}$ is constrained-Pareto stationary, there exist $\lambda \in \mathbb{R}_{\geq 0}^N$ and $\nu \in \mathbb{R}_{\geq 0}^M$ satisfying the following:

$$\sum_{i=1}^N \lambda_i \nabla J_{R_i}(\bar{\theta}) = \sum_{k=1}^M \nu_k \nabla J_{C_k}(\bar{\theta}), \quad (30)$$

where $\sum_i \lambda_i = 1$, $\nu_k = 0$ for $J_{C_k}(\bar{\theta}) < d_k$. Since $\sum_i \lambda_i = 1$, the value of λ in at least one dimension is greater than 0. Without loss of generality, we can refer to the index of such a dimension as 1. Then, the following is satisfied:

$$-\nabla J_{R_1}(\bar{\theta}) + \sum_{i=2}^N \bar{\lambda}_i (-\nabla J_{R_i}(\bar{\theta})) + \sum_{k=1}^M \bar{\nu}_k \nabla J_{C_k}(\bar{\theta}) = 0, \quad (31)$$

where $\bar{\lambda}_i = \lambda_i/\lambda_1$ for $k \geq 2$ and $\bar{\nu}_k = \nu_k/\lambda_1$. The above equation can be viewed as the stationarity condition of the KKT conditions for the following optimization problem:

$$\text{minimize}_{\theta} -J_{R_1}(\theta) \text{ s.t. } J_{R_i}(\bar{\theta}) \leq J_{R_i}(\theta) \forall i \geq 2, J_{C_k}(\bar{\theta}) \leq d_k \forall k. \quad (32)$$

Since the complementary slackness and the feasibility condition are also satisfied due to (31), all of the KKT conditions are satisfied at $\theta = \bar{\theta}$. Also, the objective and constraints of (32) are convex under the assumptions, so the policy at $\theta = \bar{\theta}$ is the optimal solution of (32). This means that the objectives cannot be improved further within the feasible region, which means the policy is constrained-Pareto optimal. As a result, if a policy is constrained-Pareto stationary, the policy is constrained-Pareto optimal. \square

Lemma A.1. *If (8) has no solution, the current policy $\pi_{\theta_{\text{old}}}$ is ϵ -CP stationary.*

Proof. Let us assume that the initial policy is feasible, which means $J_{C_k}(\theta_0) \leq d_k \forall k$. Then, the current policy also satisfies $J_{C_k}(\theta_{\text{old}}) \leq d_k \forall k$ by Theorem 4.2. We can define sets $A := \{g|\omega_i e_i \leq g_i^T g \forall i\}$ and $B := \{g|b_k^T g + J_{C_k}(\theta_{\text{old}}) \leq d_k - K\epsilon \text{ for } k \in I_{AC}^\epsilon\}$. Equation (8) has no solution means $A \cap B = \emptyset$. Since $A \supset \{g|e_i \leq g_i^T g \forall i\}$ and $B \supset \{g|b_k^T g \leq h_k := \min(d_k - K\epsilon - J_{C_k}, 0) \text{ for } k \in I_{AC}^\epsilon\}$,

$$\{g|e_i \leq g_i^T g \forall i\} \cap \{g|b_k^T g \leq h_k \text{ for } k \in I_{AC}^\epsilon\} = \{g|e_i \leq g_i^T g \forall i, -h_k \leq -b_k^T g \text{ for } k \in I_{AC}^\epsilon\} = \emptyset. \quad (33)$$

As $e_i \geq 0$ and $-h_k \geq 0$, the above equation implies that there is no direction to increase J_{R_i} and $-J_{C_k}$. If we view the CMORL problem as a modified MORL problem, where $-J_{C_k}$ is added as objectives, the current policy is Pareto optimal since there is no direction to improve all objectives. According to Theorem 1 in Désidéri (2012), there exist $\lambda \in \mathbb{R}_{\geq 0}^N$ and $\nu \in \mathbb{R}_{\geq 0}^{|I_{AC}^\epsilon|}$ such that,

$$\sum_i \lambda_i \nabla J_{R_i}(\theta_{\text{old}}) - \sum_{k \in I_{AC}^\epsilon} \nu_k \nabla J_{C_k}(\theta_{\text{old}}) = 0, \quad (34)$$

where $\sum_i \lambda_i + \sum_k \nu_k = 1$. According to Lemma A.4 in (Kim et al., 2023), the set B is not empty under the assumptions that the constraints are convex and $\{\theta|J_{C_k}(\theta) < d_k' \forall k\} \neq \emptyset$. If A is empty, there exists λ such that $\sum_i \lambda_i \neq 0$. If A is not empty, there exist λ and ν such that $\sum_i \lambda_i \neq 0$ and $\sum_k \nu_k \neq 0$ since A and B are not empty. As a result, there exist λ such that $\sum_i \lambda_i$ is positive. By redefining the multipliers as $\lambda' = \lambda/\sum_i \lambda_i$, $\nu'_{k \in I_{AC}^\epsilon} = \nu_k/\sum_i \lambda_i$, and $\nu'_{k \notin I_{AC}^\epsilon} = 0$, the current policy $\pi_{\theta_{\text{old}}}$ satisfies the ϵ -CP stationary condition. \square

Theorem 4.7. *By updating a policy using CoMOGA, the policy converges to a ϵ -CP stationary policy. Furthermore, if there is no solution to (8), the current policy is ϵ -CP stationary.*

Proof. The proof of the latter statement can be shown through Lemma A.1, so we only focus on the former statement. Since the objectives for $i \in I_\omega$ are monotonically improved according to Theorem 4.2 and are bounded by $R_{\max}/(1 - \gamma)$, the objectives will converge to specific values. At these converged values, let us assume that the policy is not ϵ -CP stationary.

Under this assumption, the solution of (8), denoted as $\bar{g}_\omega^{\text{ag}}$, must exist according to Theorem 4.2. Furthermore, the gradients of the objectives g_i are non-zero for $i \in I_\omega$. This is because if one of the gradients of the objectives are zero, the policy parameters satisfy the Pareto stationary condition by setting $\lambda_i = 1$ and $\lambda_{j \neq i} = \nu_k = 0$. Since $e_i = \epsilon g_i^T H^{-1} g_i \neq 0$ for $i \in I_\omega$, $\bar{g}_\omega^{\text{ag}} \neq \mathbf{0}$ and $g_\omega^{\text{ag}} \neq \mathbf{0}$. Then if we update the policy parameter to $\theta_{\text{new}} = \theta_{\text{old}} + g_\omega^{\text{ag}}/2 = \beta_1 \beta_2 \bar{g}_\omega^{\text{ag}}/2$, the following inequality holds:

$$J_{R_i}(\theta_{\text{new}}) - J_{R_i}(\theta_{\text{old}}) \geq \frac{\beta_1 \beta_2}{2} \left(e_i - \frac{L \beta_1 \beta_2}{4} \|\bar{g}_\omega^{\text{ag}}\|_2^2 \right) > 0. \quad (35)$$

This implies that the objective remains non-stationary, which is contrary to the convergence. Due to this contradiction, the policy at the converged values is ϵ -CP stationary. \square

B. Experimental Details

In this section, we describe the details of each task, including Safety Gymnasium, legged robot locomotion, and Multi-Objective Gymnasium. We then provide a detailed explanation of the performance metrics named hypervolume and sparsity. Finally, we present implementation details, such as network architectures and hyperparameter settings.

B.1. Task Details

B.1.1. SAFETY GYMNASIUM

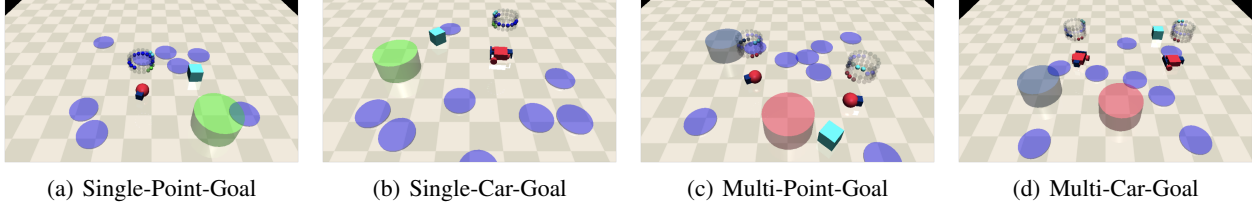


Figure 4: **Snapshots of the Safety-Gymnasium tasks.** There are two types of robots: point and car. These tasks aim to control the robots to reach goals while avoiding hazardous areas, colored purple. In the Single-Point-Goal and Single-Car-Goal tasks, a single goal, shown in green, is randomly spawned. Conversely, the Multi-Point-Goal and Multi-Car-Goal tasks have two goals, shown in blue and red, and if an agent reaches any of them, a reward is given to the agent.

In the Safety Gymnasium (Ji et al., 2023), we utilize the single-agent safe navigation tasks: `SafetyPointGoal1-v0` and `SafetyCarGoal1-v0`, and the multi-agent safe navigation tasks: `SafetyPointMultiGoal1-v0` and `SafetyCarMultiGoal1-v0`. Snapshots of each task are shown in Figure 4.

In the single-agent tasks, the observation space includes velocity, acceleration, and Lidar of the goal and hazards, and the dimensions are 60 and 72 for the point and car robots, respectively. The action space for both robots is two-dimensional. There are eight hazard areas and one goal, and hazard areas are randomly spawned at the beginning of each episode, while goals are randomly placed whenever the agent reaches the current goal. These tasks originally had a single objective: maximizing the number of goals reached. However, in order to have multiple objectives, we have modified them to include a second objective: minimizing energy consumption. Therefore, the reward is two-dimensional, and we use the original definition for the first reward (please refer to Ji et al. (2023)). The second reward is defined as follows:

$$R_2(s, a, s') := -\frac{1}{|A|} \sum_{i=1}^{|A|} (a_i/10)^2. \quad (36)$$

Also, we use the original definition of the cost function, which gives one if the agent enters hazardous areas and zero otherwise.

The multi-agent tasks have two agents and two goals, and we need to control both agents to reach goals as much as possible while avoiding hazardous areas. The original implementation uses a dictionary type for observations and actions, so we have modified them to be an array type. Additionally, in the original setup, each goal is pre-assigned to a specific agent, reducing the difficulty of solving multi-agent tasks. Therefore, we have modified the implementation so that each goal is not pre-assigned, allowing each agent to compete to achieve goals. The observation space contains the same information from the single-agent tasks for the two agents, as well as additional information: Lidar of the first and second goals. The dimensions of observation space are then 152 and 176 for the point and car robots, respectively. The action space is four-dimensional, which is doubled from the single-agent tasks to control both agents. These tasks have two objectives: maximizing the number of goals reached by each agent. Also, there are two constraints: avoiding hazardous areas for each agent. Since there are no additional objectives or constraints, the original definitions of the reward and cost functions are used without modification.

B.1.2. LEGGED ROBOT LOCOMOTION

The legged robot locomotion tasks (Kim et al., 2023) aim to control bipedal or quadrupedal robots so that their velocity matches a randomly sampled command. This command specifies the target linear velocities in the x and y-axis directions

and the target angular velocity in the z-axis direction, denoted by $(v_x^{\text{cmd}}, v_y^{\text{cmd}}, \omega_z^{\text{cmd}})$. Snapshots of these tasks are shown in Figure 5. The quadrupedal robot has 12 joints and 12 motors, and the bipedal robot has 14 joints and 10 motors. Each robot is operated by a PD controller that follows the target position of the motors, and the target position is given as an action. Hence, the number of motors corresponds to the dimension of action space. In order to provide enough information for stable control, observations include the command, linear and angular velocities of the robot base, and the position and velocity of each joint. As a result, the dimensions of the observation space are 160 for the quadruped and 132 for the biped. Originally, these tasks have a single objective of following a given command and three constraints: 1) maintaining body balance, 2) keeping the height of CoM (center of mass) above a certain level, and 3) adhering to pre-defined foot contact timing. Therefore, we use the original implementation for the observation, action, and cost functions but modify the reward function to have multiple objectives. The modified version has two objectives: 1) reducing the difference between the current velocity and the command and 2) minimizing energy consumption. Then, the reward function is defined as follows:

$$\begin{aligned}
 R_1(s, a, s') &:= 1 - (v_x^{\text{base}} - v_x^{\text{cmd}})^2 - (v_y^{\text{base}} - v_y^{\text{cmd}})^2 - (\omega_z^{\text{base}} - \omega_z^{\text{cmd}})^2, \\
 R_2(s, a, s') &:= 1 - \frac{1}{J} \sum_{j=1}^J \left(\frac{\tau_j}{M_{\text{robot}}} \right)^2,
 \end{aligned} \tag{37}$$

where J is the number of joints, τ_j is the torque applied to the j th joint, and M_{robot} is the mass of the robot. However, in the simulation of the bipedal robot, obtaining valid torque information is difficult due to the presence of closed loops in the joint configuration. To address this issue, we modify the second reward for the bipedal robot to penalize the action instead of the joint torque as follows:

$$R_2(s, a, s') := 1 - \frac{1}{|A|} \sum_{i=1}^{|A|} a_i^2. \tag{38}$$

B.1.3. MULTI-OBJECTIVE GYMNASIUM

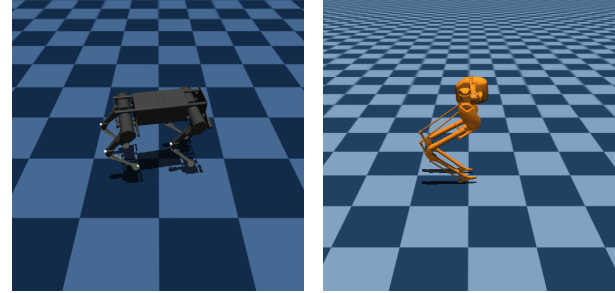
We utilize the Multi-Objective (MO) Gymnasium (Felten et al., 2023) to evaluate the proposed method in MORL tasks which have no constraints. Among several tasks, we use continuous action tasks, and there are four tasks available: `mo-hopper-v4`, `mo-halfcheetah-v4`, `mo-lunar-lander-continuous-v2`, and `water-reservoir-v0`. `mo-mountaincarcontinuous-v0` is also provided as a continuous action task in the MO Gymnasium, but we exclude it since there is an issue in the reward function. Description of the observation space, action space, and the number of objectives for these tasks are summarized in Table 4, and for more details, please refer to Felten et al. (2023).

Table 4: Specifications of MO-Gymnasium tasks.

	Observation Space	Action Space	# of Objectives (Entries)
Half-Cheetah	$\subseteq \mathbb{R}^{17}$	$\subseteq \mathbb{R}^6$	2 (velocity, energy)
Hopper	$\subseteq \mathbb{R}^{11}$	$\subseteq \mathbb{R}^3$	3 (velocity, height, energy)
Water-Reservoir	$\subseteq \mathbb{R}^1$	$\subseteq \mathbb{R}^1$	2 (excess, deficit)
Lunar-Lander	$\subseteq \mathbb{R}^8$	$\subseteq \mathbb{R}^2$	4 (success, shaping reward, main fuel, side fuel)

B.2. Metric Details

In this section, we explain in detail the performance metrics used in the main text: hypervolume (HV) and normalized sparsity ($\overline{\text{SP}}$). First, we need to prepare an estimated CP front to calculate such metrics. To do this, we pre-sample a fixed number of equally spaced preferences and roll out the trained universal policy for each pre-sampled preference to



(a) Quadruped

(b) Biped

Figure 5: **Snapshots of the legged robot locomotion tasks.** Robots aim to follow a given command while ensuring they do not fall over.

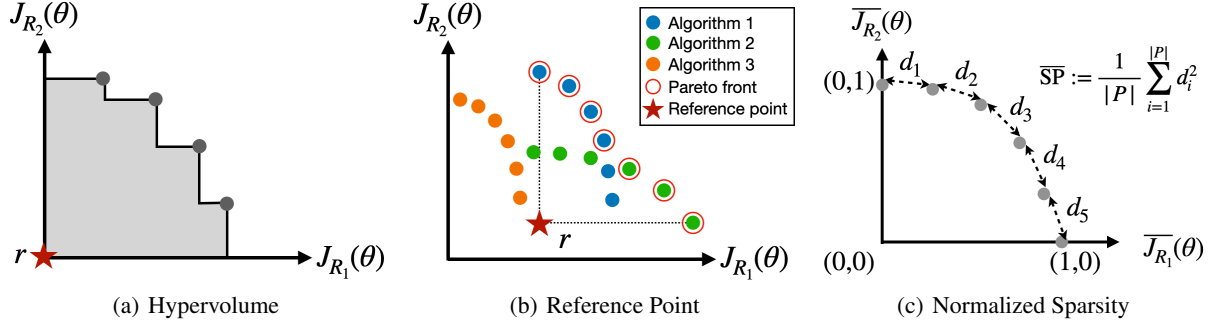


Figure 6: **Details of performance metrics.** The hypervolume is represented by the gray area in (a). In (b), the red star indicates the reference point, determined from the entire Pareto front, whose elements are circled in red. In (c), the normalized sparsity is calculated by averaging the squared distances between elements in the normalized space.

estimate objective and constraint values. If the constraint values do not exceed the thresholds, we store the objective values, $(J_{R_1}(\theta), \dots, J_{R_N}(\theta))$, in a set. Once this process is completed for all preferences, we can construct an estimated CP font by extracting elements from the collected set that are not dominated by any others. Now, we introduce details on each metric.

HV is the volume of the area surrounding a given reference point, r , and an estimated CP front, P , as defined in (14) and is visualized in Figure 6(a). However, as seen in Figure 6(a) or (14), the metric value varies depending on what reference point is used. Therefore, we do not set the reference point arbitrarily but use a method of determining the reference point from the results of all algorithms, as shown in Figure 6(b). For a detailed explanation, suppose that we have a set of estimated CP fronts, $\{P_i\}_{i=1}^K$, where P_i is the estimated front obtained from the i th algorithm. Then, we obtain the union of $\{P_i\}_{i=1}^K$, denoted by P' , and extract elements that are not dominated by any others in P' to find the Pareto front of the entire set, $\text{PF}(P')$, whose elements are circled in red in Figure 6(b). Finally, we get the reference point whose i th value is $\min(\{p_i | \forall p \in \text{PF}(P')\})$. Through this process, the reference point can be automatically set after obtaining results from all algorithms for each task. In addition, the HV value can be zero for some algorithms whose elements are entirely dominated by $\text{PF}(P')$. An example of this is Algorithm 3 in Figure 6(b).

As mentioned in the main text, sparsity (SP) has a correlation with HV. An increase in HV implies that the elements of the CP front are moving further away from each other, which increases SP. To remove this correlation, we provide a normalized version as defined in (16), and the calculation process is illustrated in Figure 6(c). Given an estimated CP front, P , we normalize each estimated objective value so that the minimum value corresponds to zero and the maximum to one. The normalized objectives are denoted as $\bar{J}_{R_i}(\theta)$. We then calculate the average of the squares of the distances between elements in this normalized space. This normalized version still produces a large value when a CP front is densely clustered in particular areas while being sparsely distributed overall. Therefore, it maintains the ability to measure sparsity while removing the correlation with HV.

B.3. Implementation Details

B.3.1. MORL TO CMORL USING THE LAGRANGIAN METHOD

In order to apply linear scalarization-based MORL methods to CMORL, it is required to solve the following constrained optimization problem given a preference ω :

$$\max_{\theta} \sum_{i=1}^N \omega_i J_{R_i}(\theta) \text{ s.t. } J_{C_k}(\theta) \leq d_k \quad \forall k \in \{1, \dots, M\}. \quad (39)$$

As explained in the main text, the constraints of the above problem can be handled by converting it into a Lagrange dual problem, and the dual problem is written as follows:

$$\max_{\lambda \geq 0} \min_{\theta} - \sum_{i=1}^N \omega_i J_{R_i}(\theta) + \sum_{k=1}^M \lambda_k \cdot (J_{C_k}(\theta) - d_k), \quad (40)$$

where λ_k are Lagrange multipliers. The multiplies should be learned separately for each preference, but preferences have continuous values. Therefore, we instead parameterize the multiplier using neural networks as $\lambda_{\phi}(\omega)$, where ϕ is a parameter.

Then, the above problem can be solved by concurrently updating the policy parameter and the Lagrange multipliers using the following loss functions:

$$\begin{aligned} \min_{\theta} L(\theta) &:= - \sum_{i=1}^N \omega_i J_{R_i}(\theta) + \sum_{k=1}^M \lambda_k J_{C_k}(\theta), \\ \min_{\phi} L(\phi) &:= - \sum_{k=1}^M \lambda_{k,\phi}(\omega)(J_{C_k}(\theta) - d_k) \text{ s.t. } \lambda_{k,\phi}(\omega) \geq 0, \end{aligned} \quad (41)$$

where the multipliers can be forced to non-negative values using some activation functions, such as softplus and exponential functions. The policy loss in (41) is constructed by adding $\sum \lambda_k J_{C_k}(\theta)$ to the loss from the unconstrained MORL problem. Therefore, the implementation of the existing MORL algorithms can be easily extended to a CMORL algorithm by adding $\sum \lambda_k J_{C_k}(\theta)$ to the original policy loss.

B.3.2. QUADRATIC PROGRAMMING PROBLEM

In the main text, we have proposed to obtain the aggregated gradient $\bar{g}_{\omega}^{\text{ag}}$ by solving the quadratic programming (QP) problem (8), which can be addressed using an existing QP solver (Goldfarb & Idnani, 1983). However, due to the large dimensions of the policy parameter space where the problem is defined, it will take a long time to calculate the aggregated gradient. As an alternative, we propose to solve a Lagrange dual problem. Given that QP problems hold strong duality, the solution to the dual problem is equivalent to that of the original problem. The dual problem is then expressed as follows:

$$\max_{\lambda \geq 0, \nu \geq 0} \min_g \frac{1}{2} g^T H g + \sum_{i=1}^N \lambda_i (\omega_i e_i - g_i^T g) + \sum_{k \in I_{\text{AC}}^c} \nu_k (b_k^T g + J_{C_k}(\theta_{\text{old}}) - d'_k) =: L(g, \lambda, \nu), \quad (42)$$

where λ and ν are Lagrange multipliers. Since $\text{argmin}_g L(g, \lambda, \nu)$ is $H^{-1}(\sum_i \lambda_i g_i - \sum_k \nu_k b_k)$, denoted by $g^*(\lambda, \nu)$, we can get the following problem by replacing g with $g^*(\lambda, \nu)$:

$$\begin{aligned} \min_{\lambda \geq 0, \nu \geq 0} & \frac{1}{2} \sum_{i=1}^N \sum_{j=1}^N \lambda_i \lambda_j g_i^T H^{-1} g_j + \frac{1}{2} \sum_{i \in I_{\text{AC}}^c} \sum_{j \in I_{\text{AC}}^c} \nu_i \nu_j b_i^T H^{-1} b_j - \sum_{i=1}^N \sum_{j \in I_{\text{AC}}^c} \lambda_i \nu_j g_i^T H^{-1} b_j \\ & - \sum_{i=1}^N \lambda_i \omega_i e_i - \sum_{k \in I_{\text{AC}}^c} \nu_k (J_{C_k}(\theta_{\text{old}}) - d'_k), \end{aligned} \quad (43)$$

where $g_i^T H^{-1} g_j$, $b_i^T H^{-1} b_j$, and $g_i^T H^{-1} b_j$ can be computed in parallel using GPU. We have formulated the new QP problem (43) in the dual space of dimension $N + |I_{\text{AC}}^c| \leq N + M$, which is much smaller than the dimension of the policy parameter space. Now, we solve (43) using a QP solver to get the optimal dual variables, which are denoted by λ^* and ν^* . Finally, the aggregated gradient can be expressed as follows using the optimal dual variables:

$$\bar{g}_{\omega}^{\text{ag}} = \sum_{i=1}^N \lambda_i^* H^{-1} g_i - \sum_{k \in I_{\text{AC}}^c} \nu_k^* H^{-1} b_k. \quad (44)$$

B.3.3. NETWORK ARCHITECTURE

The proposed method and baselines are based on the actor-critic framework, requiring policy and critic networks. Additionally, since the baselines use the Lagrangian method to handle the constraints, they use multiplier networks, as mentioned in Appendix B.3.1. We have implemented these networks as fully connected networks (FCNs), and their structures are presented in Table 5. In the unconstrained tasks, MO-Gymnasium, we use standard critic networks that output scalar values for given observations and preferences. However, the standard critic networks usually estimate the objective or constraint functions with large biases, making it challenging to satisfy the constraints. Therefore, we use quantile distributional critics (Dabney et al., 2018) to lower the estimation biases in the Safety-Gymnasium and legged robot locomotion experiments. The quantile distribution critic outputs several quantile values of the discounted sum of the reward or cost functions for given observations and preferences. Then, the objective or constraint functions can be estimated by averaging the outputted

Table 5: Network structures.

	Parameter	Value
Policy network	Hidden layer	(512, 512)
	Activation	LeakyReLU
	Normalization	✗
Critic network	Hidden layer	(512, 512)
	Activation	LeakyReLU
	Normalization	✗
Quantile distributional critic network	Hidden layer	(512, 512)
	Activation	LeakyReLU
	Normalization	LayerNorm
	# of quantiles	25
Multiplier network	Hidden layer	(512,)
	Activation	LeakyReLU
	Normalization	✗

quantiles. For the proposed method and LP3 that have similar frameworks to TRPO (Schulman et al., 2015), we use the TD(λ) method (Kim et al., 2023) to train the distributional critic networks. For PD-MORL and CAPQL, the distributional critic networks are trained by reducing the Wasserstein distance between the current quantiles and the truncated one-step TD targets, as in TQC (Kuznetsov et al., 2020). The policy network, similar to other RL algorithms dealing with continuous action spaces (Schulman et al., 2015; Haarnoja et al., 2018; Fujimoto et al., 2018), outputs the mean and diagonal variance of a normal distribution. However, in the locomotion tasks, the policy networks are modified to output only the mean value by fixing the diagonal variance in order to lower the training difficulty.

B.3.4. HYPERPARAMETER SETTINGS

We report the hyperparameter settings for the CMORL tasks (Safety-Gymnasium, Locomotion) in Table 6 and the settings for the MORL tasks (MO-Gymnasium) in Table 7.

Table 6: Hyperparameters for CMORL tasks.

	CAPQL	PD-MORL	LP3	CoMOGA (Ours)
Discount factor	0.99	0.99	0.99	0.99
Length of replay buffer	1000000	1000000	100000	100000
Steps per update	10	10	1000	1000
Batch size	256	256	10000	10000
Optimizer	Adam	Adam	Adam	Adam
Policy learning rate	3×10^{-4}	3×10^{-4}	-	3×10^{-4}
Critic learning rate	3×10^{-4}	3×10^{-4}	3×10^{-4}	3×10^{-4}
Multiplier learning rate	1×10^{-5}	1×10^{-5}	3×10^{-4}	-
Soft update ratio	0.005	0.005	-	-
# of quantiles to truncate	2	2	-	-
# of HER samples	-	3	-	-
Angle loss coefficient	-	10	-	-
Explore and target action noise scale	-	(0.1, 0.2)	-	-
# of action samples	-	-	20	-
TD(λ) factor	-	-	0.97	0.97
# of target quantiles	-	-	50	50
# of preference samples	-	-	10	3
Local region size	-	-	0.05	0.05
K	-	-	-	0
G	-	-	-	∞
H matrix	-	-	Hessian of KL divergence	Hessian of KL divergence

Table 7: Hyperparameters for MORL tasks.

	CAPQL	PD-MORL	LP3	CoMOGA (Ours)
Discount factor	0.99	0.99	0.99	0.99
Length of replay buffer	1000000	1000000	100000	1000000
Steps per update	1	1	1000	10
Batch size	256	256	10000	256
Optimizer	Adam	Adam	Adam	Adam
Policy learning rate	3×10^{-4}	3×10^{-4}	-	3×10^{-5}
Critic learning rate	3×10^{-4}	3×10^{-4}	3×10^{-4}	3×10^{-4}
Soft update ratio	0.005	0.005	-	0.005
# of HER samples	-	3	-	-
Angle loss coefficient	-	10	-	-
Explore and target action noise scale	-	(0.1, 0.2)	-	-
# of action samples	-	-	20	-
TD(λ) factor	-	-	0.97	-
# of preference samples	-	-	10	10
Local region size	-	-	0.14	0.1
K	-	-	-	0
G	-	-	-	∞
H matrix	-	-	Hessian of KL divergence	Identity matrix

C. Additional Experimental Results

In this section, we introduce and analyze the results of ablation studies on the hyperparameters of the proposed method. Next, the performance metrics of the experiment presented in Section 6.5, which compares the proposed method with the LS version, are reported. Lastly, we visualize the estimated CP fronts for tasks with two objectives.

C.1. Ablation Study on Hyperparameters

The proposed method has introduced new hyperparameters, ϵ , K , and G . We first describe the role of each hyperparameter and show the results of the ablation study. ϵ is the local region size, where the local region is defined as $\|\Delta\theta\|_H \leq \epsilon$. Since ϵ adjusts the size of the policy update, it serves as the learning rate of the policy parameter. K is introduced in (8) to mitigate the risk of constraint violation arising from linear approximation, and this is achieved by reducing the threshold by $K\epsilon$. Therefore, setting a large K lowers the likelihood of constraint violations. However, assigning a too large value to K can lead to an empty feasible region, $\{\theta | J_{C_k}(\theta) \leq d_k - K\epsilon\} = \emptyset$, causing the policy to break down. G is introduced to scale down the policy gradient when α defined in (9) becomes large. α is defined as the ratio of the magnitude of the aggregated gradient $\bar{g}_\omega^{\text{ag}}$ to that of each objective’s gradient. Consequently, α increases when the gradients of the objectives are in opposing directions, indicating a gradient conflict. Thus, G serves to reduce the size of the policy gradient in such conflict situations. From this observation, a smaller G implies a strict judgment of gradient conflicts, while a larger G indicates a generous judgment of these conflicts.

Now, we introduce the ablation study on the hyperparameters. We conduct experiments on the quadrupedal task in the legged robot locomotion environment for various hyperparameter values. In particular, we also conduct the experiments at $K = 0$, a setting that does not reduce the thresholds of the constraints, and $G = \infty$, a setting that does not consider gradient conflicts. The results of the ablation study are reported in Table 8, and trends in HV and SP values according to hyperparameter values are visualized in Figure 7. Table 8 confirms that the constraints are satisfied in all settings, and Figure 7 shows that the performance metric values do not change significantly across all settings. However, a significant performance drop is observed at $K = 100$, which is likely because a huge K causes the feasible region to become empty, causing the policy to be updated in the wrong direction, as mentioned earlier. We also see a slight decrease in HV for $G = 1$, which is due to the strict judgment of gradient conflicts, making the policy updated conservatively. Except for these settings, there is no significant change in performance according to the hyperparameter settings, including $K = 0$, which does not reduce the thresholds, and $G = \infty$, which does not consider gradient conflicts. From this observation, we recommend setting $K = 0$ and $G = \infty$ to reduce the complexity of hyperparameter tuning. Also, we have conducted the main experiments with $K = 0$ and $G = \infty$, as observed in Appendix B.3.4.

Table 8: **Results of the ablation study on the hyperparameters.** The reported values are obtained by averaging results from five random seeds.

	Trust region size, ϵ				K				G			
Value	0.01	0.02	0.05	0.1	0.0	1.0	10.0	100.0	1	10	100	∞
HV ($\times 10^4$) \uparrow	4.736	4.676	4.840	4.765	4.839	4.915	4.920	0.000	4.064	4.829	4.872	4.839
\overline{SP} ($\times 10^{-2}$) \downarrow	1.643	1.795	1.691	2.496	1.691	2.799	2.009	159.884	1.810	1.746	1.917	1.691
Con1 (≤ 0.025)	0.005	0.005	0.015	0.012	0.015	0.006	0.008	0.024	0.003	0.004	0.008	0.015
Con2 (≤ 0.025)	0.003	0.003	0.014	0.012	0.014	0.004	0.004	0.006	0.002	0.001	0.006	0.014
Con3 (≤ 0.4)	0.322	0.326	0.338	0.340	0.338	0.324	0.320	0.329	0.300	0.291	0.325	0.338

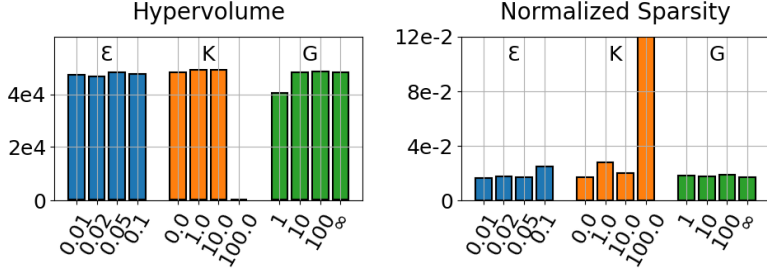


Figure 7: Trends in HV and SP according to hyperparameter settings.

C.2. Performance Metrics of Experiments in Section 6.5

We report the performance metric values of the experiments which compare the proposed method with the linear scalarization (LS) version, conducted in Section 6.5. The results are presented in Table 9.

Table 9: **Experimental results comparing the proposed method with LS version.** The reported values are obtained by averaging results from five random seeds.

	CoMOGA (Ours)			Linear Scalarization		
Scale of the energy efficiency objective	$\times 10.0$	$\times 1.0$	$\times 0.1$	$\times 10.0$	$\times 1.0$	$\times 0.1$
HV ($\times 10^4$) \uparrow	5.823	5.941	5.886	5.205	5.942	4.690
\overline{SP} ($\times 10^{-2}$) \downarrow	2.010	1.691	2.478	5.001	1.404	5.516
Con1 (≤ 0.025)	0.016	0.015	0.012	0.006	0.007	0.017
Con2 (≤ 0.025)	0.007	0.014	0.007	0.014	0.003	0.007
Con3 (≤ 0.4)	0.336	0.338	0.326	0.340	0.309	0.315

C.3. Visualization of Estimated CP Fronts

As mentioned in Appendix B.2, we can obtain the estimated CP front from the trained universal policy. We use 20 equally spaced preferences to get the fronts for each task, and the obtained CP fronts are visualized in Figure 8. The hopper and Lunar-Lander tasks in the MO-Gymnasium are excluded from this visualization as they have three and four objectives, respectively.

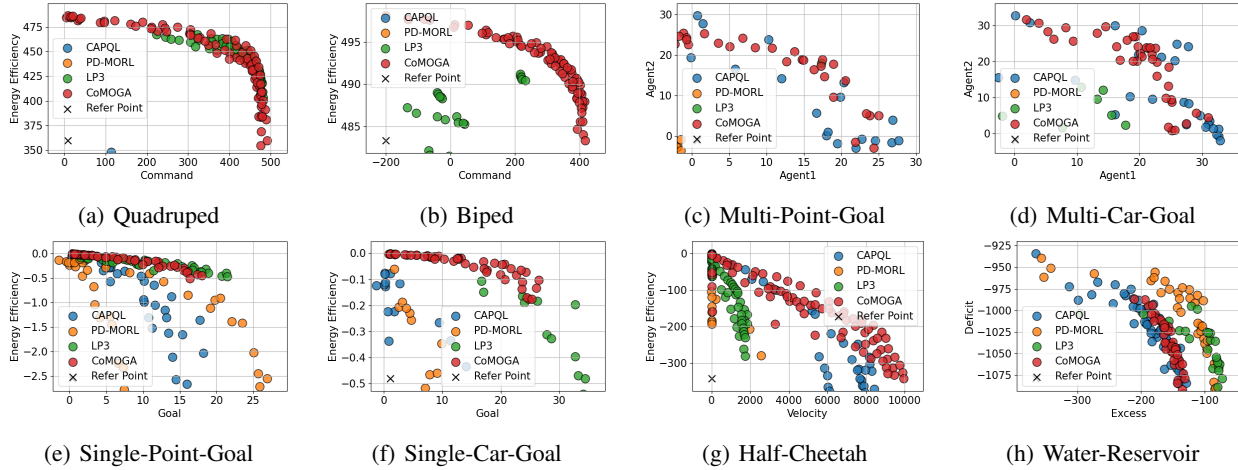


Figure 8: **Visualization of Estimated CP Fronts.** For each task, we plot the estimated fronts obtained from five random seeds in the same figure. The number of items in the fronts can be reduced due to constraint violations or non-dominant policies.